Applied Materials Today 21 (2020) 100835

Contents lists available at ScienceDirect

Applied Materials Today

journal homepage: www.elsevier.com/locate/apmt

Indium tin oxide nanowires manufactured via printing and laser irradiation

J.R. McGhee[a,*], A. Goulas[b], D.J. Southee[a], J.S. Sagu[c], D.S. Engstrøm[b], J. Wang[b], D.A. Hutt[b], P.S.A. Evans[a,c], Z. Zhou[d], K.G.U. Wijayantha[c], P. Conway[b], C.J. Carmalt[e]

[a] Design Research for Additive Manufacturing Lab, Loughborough University Design School, Loughborough University, Loughborough, Leicestershire, LE11 3TU, UK
[b] Wolfson School of Mechanical, Electrical and Manufacturing Engineering, Loughborough University, Loughborough, Leicestershire, LE11 3TU, UK
[c] Energy Research Laboratory, Department of Chemistry, Loughborough University, Loughborough, Leicestershire, LE11 3TU, UK
[d] Loughborough Materials Characterisation Centre, Department of Materials, Loughborough University, Loughborough, Leicestershire, LE11 3TU, UK
[e] Materials Research, Department of Chemistry, University College London, London WC1E 6BT, UK

ARTICLE INFO

Article history:
Received 12 August 2020
Revised 9 September 2020
Accepted 15 September 2020

Keywords:
Transparent conducting oxides
Laser processing
Printed electronics manufacturing
Additive manufacturing
Indium tin oxide
Nanostructures

ABSTRACT

Metallic and semiconductor nanowires can provide dramatically increased electrical and optical properties in a wide range of fields, ranging from photovoltaics to sensors and catalysts. In this research, a rapid manufacturing process has been developed for printing indium tin oxide microparticles and converting them into nanowires. Microparticle indium tin oxide (ITO) inks were formulated and printed. These were then converted into hierarchical nanowire films via laser irradiation (980 nm, NIR) with raster speeds of 40 mm s^{-1} in air, much faster compared to traditional manufacturing processes. For a 4 cm^2 film, only 40 s of processing were required. A full materials characterization was performed on the materials pre and post laser processing with the most probable conversion mechanism found to be a laser induced carbothermal reduction process. Microstructural, chemical, and crystallographic evidence of the laser induced carbothermal reduction process were derived from SEM, XRD, XPS and TEM analysis. Compared to conventionally heat-treated printed samples, laser processing was found to increase the conductivity of the printed ITO from 0.88% to 40.47% bulk conductivity. This research demonstrates the ability of printing and laser processing to form nanowires in a high-speed manufacturing context, thereby enabling the development of printed non-transparent ITO nanowire electronics and devices.

1. Introduction

Nanostructures can be defined as particles or systems which are smaller than 100 nm in two or three dimensional axes. Nanostructures such as nanowires, nanorods and tetrapods can provide improved functionality to a wide range of extremely useful electronic materials and are of great interest to fields such as photonics, transistors, quantum computing and sensors [1–8]. Developing and fabricating semiconductor material-based nanowires and nanorods is of vital importance for the development of more advanced electronic systems [9–11]. Indium tin oxide (ITO) is one of the most widely used conducting metal oxides, and ITO based nanostructures and dendritic nanostructures are of great interest due to their excellent electrical and mechanical properties [12–13]. ITO nanostructures have the potential to provide advances in transparent conductive films, energy storage, thermoelectric devices, and even neural interfacing [14–17]. Other, similar materials, such as zinc oxide (ZnO) and doped ZnO nanostructures are currently a major field of research, demonstrating potential in high efficiency solar cells, sensors for electronic skins, UV light emitting diodes and UV laser arrays [18–21]. One of the major areas for these materials and nanostructures is in sensing devices, printed and flexible applications in particular. The optical transparency characteristic of ITO, often utilized in applications, is not an important factor in this context for sensing, with thick, porous films being preferred [22–24]. For sensors, resistive, thick film nanostructures are desirable as they allow for the improved sensing performance demonstrated in the wider literature. While a process which allows for altering the resistivity simultaneously also removes the need for bulky additional signal amplification components (e.g. Wheatstone bridge, instrumentation amplifiers) in the application, enabling, low pro-

* Corresponding author at: Wolfson School of Mechanical, Electrical and Manufacturing Engineering, Loughborough University, Loughborough, UK.
E-mail address: j.mcghee@lboro.ac.uk (J.R. McGhee).

https://doi.org/10.1016/j.apmt.2020.100835

file, printed electronics for IoT applications [25]. However, traditional manufacturing methods for metal oxide films are not well suited to exploiting the excellent sensing properties of the materials and therefore, the development of rapid manufacturing techniques for nanostructures is required. Large scale, rapid manufacturing of both powders and thin and thick films is currently a major challenge and area of research seeking to address high temperatures and the inherent time-consuming nature of traditional fabrication methods [26]. Nanostructures can be fabricated via two routes, top-down or bottom-up. Top-down processes focus on the removal of material to form nanostructures such as nanowires. Both nanolithography and milling can be used, these require the presence of a bulk film of material and etching to form highly controllable arrays of structures. Bottom-up fabrication generally involves either the most common process, vapor deposition or solution processing methods for the creation of continuous films, for example through vapor-liquid solid (VLS) nanowire growth [27]. These films can then be patterned via etching or laser ablation [28].

However, recent methods also involve reduction reactions by mixing the metal oxide powder with graphite [29]. These carbothermal reduction reactions are common in extractive metallurgy for the reduction of metal oxides into metal form such as the addition of coke in the iron ore smelting process. In this reaction, when mixtures of carbon and metal oxides are heated, the carbon acts as a reducing agent, liberating the oxygen from the metal and converting it into pure metal and CO_2 [29]. In recent years, this carbothermal reduction process has become more sophisticated and has been demonstrated to provide a route to fabricating metal oxide nanostructures from both zinc oxide and indium tin oxide [30]. This is performed by the addition of carbon (typically graphite) into both vapor deposition processes such as aerosol assisted chemical vapor deposition or mechanically mixing carbon, placing on substrates and reacting in a furnace at high temperatures (typically >1100°C for ZnO) for extended periods of time. The CO and CO_2 by-products can react again with the metal to grow metal oxide nanostructures [31]. Both fabrication processes suffer from two disadvantages, the first is the reaction time which typically ranges from 2 to 24 h. The second is that patterning the nanostructure films requires additional post-processing steps, typically via lithography.

In this work, we demonstrate, for the first time, a novel process which involves the patterning of indium tin oxide material films via Direct Ink Writing and then the fabrication of ITO nanostructures within the films by a laser induced carbothermal reduction process, carried out in air at atmospheric pressure. It is demonstrated that with the high loading of carbon within the printable ITO inks developed (30 wt.% of organics), that laser irradiation can provide enough energy to cause what data suggests is a carbothermal reduction process. This enables the conversion of printed patterns of ITO microparticles into structures containing nanowires and nanorods in seconds rather than hours. This work provides a foundation for the further development of high throughput, non-clean room manufacturing of nanostructured materials and provides a rapid manufacturing method for industries developing applications with nanostructured semiconductors.

2. Materials and methods

Commercial indium tin oxide (ITO, 99.99%, Alfa Aesar, < 25 μm particle size) was used. Inks were prepared using an EXAKT 50 L three roll mill using a nitrocellulose based polymeric resin. To formulate the ink, approximately 70wt% of ITO microparticles were mixed into 30wt% of a vehicle solution comprising of nitrocellulose, alpha terpineol and methoxy–propanol. This formulation was used as it has been demonstrated in the literature to be compatible with the high throughput, screen printing process while also being compatible with micro-dispensing [32]. Ink viscosity and rheology measurements were taken using a Haake VT550 cone and plate viscometer using the PK2, 1° cone and plate configuration. Printing/dispensing and laser processing experiments were carried out using an OurPlant XTec system (Häcker Automation GmbH, Schwarzhausen, Germany) equipped with a DX-30 syringe dispensing module and using 3 mL syringe barrels fitted with 254 μm diameter tapered tips (Nordson EFD, Aylesbury, United Kingdom). The syringe dispensing module, is a plunger based system which dispenses material through contact based printing onto the substrate. The substrates used were soda lime glass slides (Thermo Scientific, 24 × 24 × 1 mm). The optimized printing parameters for the ink were a printing pressure of 0.39 mm and a flow rate of 0.2 μLs^{-1}, from these parameters, the system automatically dictates print speed. Within the same system, a Coherent-DILAS InGaAs fiber-coupled multimode diode laser (DILAS Diode laser GmbH, Mainz, Germany), operating at a wavelength of 980 ± 10 nm, producing a beam of 330 μm diameter was used to process the printed materials.

Sheet resistance measurements of the films were taken using a Jandel HM20 four-point probe and two-point resistance measurements were taken using a Fluke-179 digital multimeter. Measurements of optical properties were recorded using a Perkins Elmer Lambda 35 UV/VIS spectrophotometer between 385 and 1100 nm with a 99.9% reflectance standard (Labsphere Spectralon). X-ray diffraction (XRD) patterns were recorded using a Bruker D2 Phaser X-ray Powder Diffractometer. The XRD patterns measured used primary monochromatic high intensity Cu K-α (λ = 1.541 Å) radiation with an acquisition time of 12 h with an incident angle (2θ) between 10 and 80°. Scanning electron microscopy images were taken on a Jeol 7800F field emission gun scanning electron microscope (FEG-SEM). The accelerating voltage used for all SEM images was 5 kV, using a typical working distance of 10 mm. Energy dispersive x-ray spectroscopy (EDX/EDS) measurements were carried out with the same Jeol 7800F FEGSEM at 20 kV, but with the working distance changed to 5 mm and software processing performed using Oxford Instruments AZTEC. X-ray photoelectron spectroscopy (XPS) data was collected using a Thermo Scientific™ K-Alpha™ XPS System utilizing an Al Kα X-ray source and data processing was performed on the Thermo Scientific™ Avantage Software. TEM characterization was undertaken using a FEI Tecnai F20 S/TEM with equipped with an Oxford Instruments X-MAX 80 TLE windowless EDX detector. TEM specimens were prepared by scratching particles off into isopropanol solvent from the laser process sample's surface to form a suspension, followed by standard drop-casting the suspension onto a holey carbon film supported TEM grid.

3. Printing and fabrication of indium tin oxide nanostructures

Indium tin oxide (ITO) tracks (20 mm long) and square films (20 × 20 mm) approximately 100 μm thick (100 μm dispensing height) were printed by micro-dispensing ITO ink (70 wt% ITO, 30 wt% nitrocellulose-based vehicle) onto soda-lime glass before laser processing (Fig. 1). A major benefit of both the printing and laser processing methods employed is they are compatible with fabrication on flexible polymer substrates.

Control samples of the printed films were also cured using conventional heating methods at temperatures that would also be compatible with flexible substrates (<240°C). The inks displayed shear thinning behavior with a viscosity (η) of 38,194 mPa.s measured at a shear rate (γ) of 2.580 s^{-1}. At a high shear rate (γ = 258.1) this viscosity was 1434 mPa.s. Data showing the viscosity versus shear rate and the shear stress of the material versus shear rate can be seen in Fig. S1 (Supplementary Information). Thermogravimetric and differential scanning calorimetry

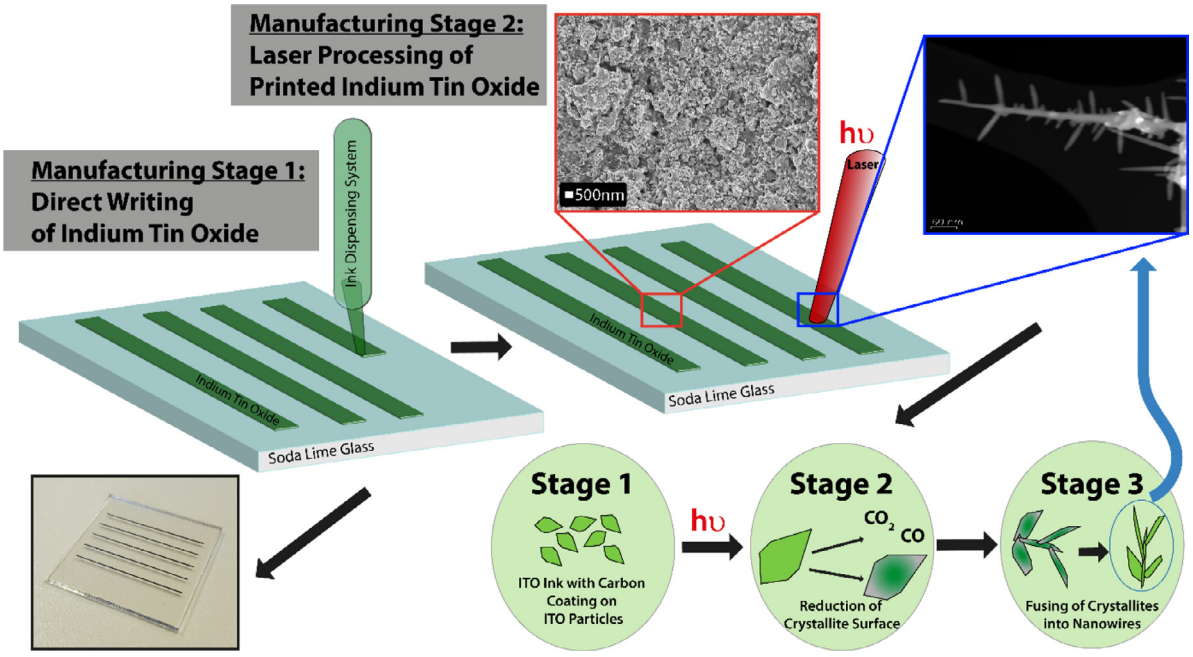

Fig.. 1. A schematic of the ITO ink printing and laser processing steps. The FEGSEM image highlighted in red displays the ITO structure before laser processing and the TEM image highlighted in blue shows a nanowire formed through laser processing. The proposed growth mechanism stages of the ITO nanowires are also shown.

(TGA/DSC) measurements were taken of the nitrocellulose vehicle (Fig. S2) to determine suitable oven curing temperatures and times. As a result of this, the control samples were oven-cured at 110°C for 10 min to enable the characteristics of the initial powder to be determined. Control samples were also heated at higher temperatures, closer to those used to sinter materials, but even with controlled binder burnout of the film up to 650°C (1°C min^{-1}) no conductivity was observed and the film would no longer adhere to the substrate.

Before laser processing, the control samples were characterized and in the displayed data figures will be referred to as the 0 W sample. The absorbance and transmission of the ITO thick films were measured via UV/VIS spectroscopy by measuring the percentage transmittance and reflectance versus a reflectance standard (99.9%, Labsphere Spectralon). The absorbance of the ITO control samples at 980 nm (the wavelength of the laser to be used) was found to be 93.98%. Although the purpose of printing the ITO is to exploit the properties of the metal oxide in non-transparent applications (sensors, electromagnetic devices etc.), ITO is also traditionally used as a transparent conductor. Due to this, the percentage transmission was measured and found to be 5.35% at 550 nm. For the control samples, the average sheet resistance was measured to be 144.6 Ω sq^{-1}. Pellets of the ITO powder were annealed at 650°C, giving a reference bulk resistivity of 7.04×10^{-3} Ω.cm measured via four-point probe to allow for a calculation of the control sample's bulk conductivity. The percentage bulk conductivity is a measure typically used in printed electronics in order to determine how close the conductivity of a printed film is to its traditionally manufactured counterpart. The bulk conductivity for the printed control samples were measured to be 0.88% the value of the conductivity of the pellet. X-ray diffraction patterns were acquired for the control samples, indicating pure, single phase ITO (PDF 93–231–0010) shown and discussed later as the 0 W pattern in Fig. 3(b).

For this ink, processing parameters were optimized by printing 32 combinations with five replicas each of varying laser powers, laser speeds and number of laser passes. A single laser pass at 40 mm s^{-1} provided the best thick film conductivity with all samples tested and, these parameters were therefore kept constant with only the laser power varied. Processing powers were kept between 2.5 and 15 W for the ITO samples. Films processed at 20 W or above absorbed too much energy for reliable sample fabrication. The laser processing was performed immediately after printing on the still wet film at room temperature, requiring no drying step in-between. The solvent used in the ITO printing inks, methoxy propanol, provides slower room temperature drying properties compared to lower molecular weight ether alternatives. This enables consistent manufacturing with minimal ink composition change pre-laser processing.

4. Experimental analysis of laser processed printed indium tin oxide films

Field emission gun scanning electron microscope (FEG-SEM) analysis of the samples, indicated that the laser process had a significant effect on the film morphology as shown in Fig. 2 (a–d). Lasers, particularly the Gaussian profiled InGaAs 980 nm diode laser used for this research, typically have a distribution of energy across the beam, with the highest energy density forming in the center, and the edges of the beam lower in intensity. Due to this, a 50 μm laser beam spot overlap was applied into the parameters for laser processing. For ITO ink films, an analysis of processing homogeneity was performed via SEM/EDX (Fig. S3). It was found that the laser created ridges in the film with different levels of porosity due to the variation in the beam intensity profile, however, the ITO composition remained consistent across the film.

Upon analyzing the SEM data in Fig. 2 (a–c), it is apparent that two stages of film conversion occur. The first stage was achieved by increasing laser power from 0 up to 7.5 W. With this increase in power, the ITO particles seen in Fig. 2(a) break up into smaller particles to form dendritic and fractal structures (Fig. 2(b)). The second stage which is shown in Fig. 2(c) is that increasing from 7.5 to 15 W these fine particles start to grow primarily into nanowires with fine particles also forming. This wire growth begins at a 10 W laser power (Fig. S4) and further growth in both wires and fine particles takes place with an increased power. In Fig. 2(d), the dif-

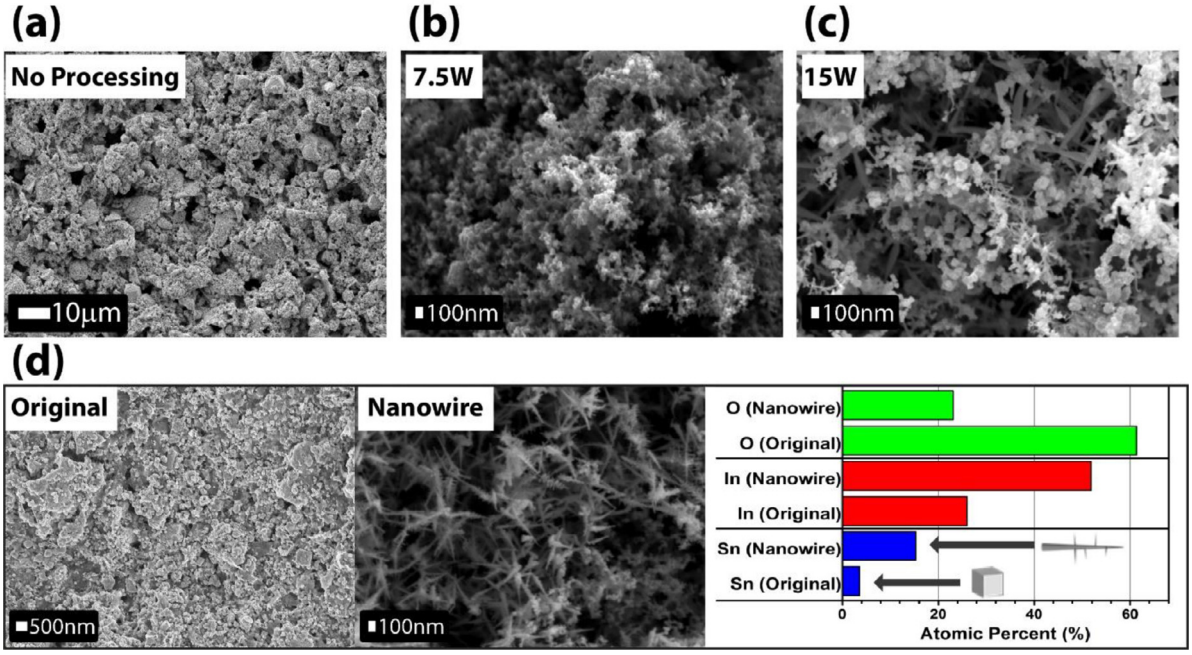

Fig.. 2. Scanning electron micrographs displaying (a) the structure of an oven cured control sample of ITO ink, (b) the structure of ITO ink processed at 7.5 W, (c) the structure of the ITO ink processed at 15 W and (d) scanning electron micrographs of the control sample compared to a processed 10 W nanowire sample with EDX analysis.

ference in the original and processed particles can be seen with the associated EDX mapping data. This data displays a decrease in oxygen content for the laser processed ITO indicating that a reduction of the metal oxides has taken place.

For each of the 4 cm^2 film samples, sheet resistance measurements shown in Fig. 3(a) were taken of both the oven cured control samples and laser processed samples. Each sample had nine sheet resistance measurements taken with each point in the figure displaying the average sheet resistances across the films and the standard deviation providing insight into film uniformity. The nine measurements were taken in a 3 × 3 grid on square prints in order to determine corner to corner uniformity with an example shown in Fig. S5. As mentioned in a previous section, to provide a reference for bulk material resistivities, pellets of the ITO powder were annealed at 650°C, giving a reference bulk resistivity of 7.04 × 10^{-3} Ω.cm measured via four-point probe. Profilometry measurements of laser processed films were taken to gather film thickness, with bulk resistivity being calculated by multiplying the sheet resistance by the film thickness. Oven cured control samples of ITO films were found to provide an average of 0.88% of the bulk conductivity. With the low laser power of 2.5 W the film was only 1.83% of the bulk conductivity. However, laser processing powers of 5 W were found to provide a large increase, reaching 40.47% of bulk conductivity. Further increasing the power caused the sheet resistance to increase slightly with nanowire growth. Nanowires created from the 15 W process displayed a mean decrease in sheet resistance for the film. However, as can be seen in the error bars, film uniformity decreases with some parts of the film demonstrating sheet resistance values as low as 3 Ω sq^{-1}. The transmission properties of the films were slightly improved post laser processing, with the 10 W film increasing from 5.35% to 10.29% at 550 nm.

Initially, a laser treatment performed at 2.5 W leads to an increase in the sheet resistance. This is associated with the laser only producing its maximum power after a rise and fall time delay, essentially curing the ink to a lesser degree than the control sample. At 5 W the most conductive films are created with an average sheet resistance of 15 Ω sq^{-1} being formed. Upon further analysis via Hall Effect measurements, the laser was found to provide the film with an increase in carrier concentration of 1.33 × 10^{19} cm^{-3} and the highest average mobility of all processed films at 31.3 cm^2 Vs^{-1}. Between 5 and 10 W sheet resistances and film uniformity is improved while at the highest power, film uniformity becomes worse with sheet resistance ranging between 3 Ω sq^{-1} and 1.07 MΩ sq^{-1} due to laser ablation of material creating a non-uniform layer thickness. As nanowires begin to form, a large drop in carrier mobility is observed which is associated with smaller crystallite size. For nanowires formed at 15 W, the carrier concentration decreases with electron mobility increasing. This is associated with a less dense film with larger crystallites being present and indicates nanowire growth with single crystal properties. By tuning the laser power for processing the material, two different structures can be formed, the first of which is the denser, dendritic and highly conducting film as seen in Fig. 2(c). Increasing this power even further allows for the second pathway towards the fabrication of indium tin oxide nanowires as seen in Fig. 2(d), however, these form at the expense of the denser, more conductive film. While this second pathway increases the sheet resistance, the 10 W nanowire samples had a uniform sheet resistance of 42 Ω sq^{-1} which is drastically improved over the control samples. This data indicates that during manufacturing using this route, the final properties of the film can be tuned, whether the lower sheet resistance of 5 W processing powers are required or a higher sheet resistance, nanowire film processed at 10 W is desired.

X-ray diffraction (XRD) patterns were recorded for the printed and processed films to determine any changes in crystal structure with laser process power (Fig. 3(b)). XRD analysis of the control samples shows single phase of ITO (PDF 93–231–0010). However, after laser processing at any power level, trace amounts of indium can be seen alongside single phase ITO (PDF 93–231–0010), as highlighted in red in the enlarged image of Fig. 3(b) and supplementary information (Fig. S6). Tin metal could not be seen in the XRD analysis, however, due to the 10:90 ratio of tin oxide to indium oxide, it is possible that tin metal is present but in amounts below the limit of detection of the x-ray diffractometer. A relative intensity change in some of the XRD peaks is also seen with increasing laser power. At powers where nanowires begin to form

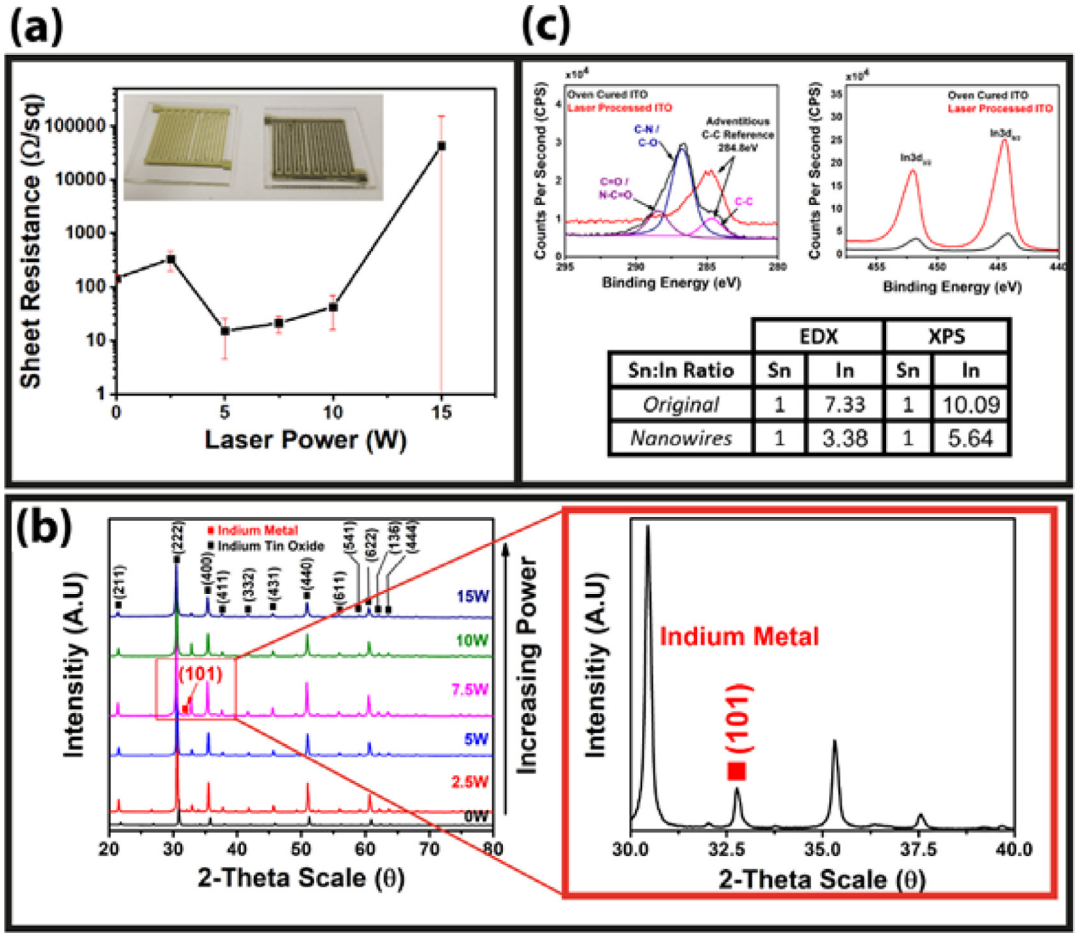

Sn:In Ratio	EDX Sn	EDX In	XPS Sn	XPS In
Original	1	7.33	1	10.09
Nanowires	1	3.38	1	5.64

Fig.. 3. Sheet resistance of ITO films versus laser power with examples of printed (left) and processed (right) films shown in the insets, (b) X-ray diffraction patterns for indium tin oxide processed at various laser powers displaying an enhanced diffraction pattern displaying trace amounts of reduced indium oxide in the form of indium metal and (c) high resolution XPS data for carbon and indium including a table comparing EDX and XPS analysis of Sn:In ratios and.

(e.g. 7.5 – 15 W) there is a 10% increase in the ratio between the (222) and (400) plane which is typically associated with an increasing level of oxygen vacancies in the ITO crystallites [33]. This again provides evidence that the laser treatment is causing a reduction within the material. It also indicates that the individual particles become more conductive as this growth in the (400) plane, combined with increasing deficiency in oxygen has been associated with an increase in ITO conductivity and quality. Therefore, the reduction in conductivity shown in Fig. 3a can be associated with a less dense film decreasing electrical percolation rather than a decrease in material quality.

X-ray photoelectron spectroscopy (XPS) was performed on an oven cured ITO ink and a laser processed nanowire specimen (15 W processing power) to determine any compositional changes to the material. Survey scans were along with high resolution scans performed for O1s, C1s, Sn3d, In3d and InMN1 regions (Fig. S7) referenced to the carbon 1 s peak as 284.8 eV. High resolution scan data for both the carbon and In3d regions are shown in Fig. 3(c). Comparing the two samples shows large differences between them. The oven cured sample retains a significant amount of binder that leads to components of the C1s envelope that can be attributed to C–N, C–O, C=O and N–C=O. Furthermore, the In3d peak intensity is low due to attenuation of the signal by the overlying binder material. It is clear that after laser processing, that the main carbon contribution is due to C–C bonds and the remaining carbon on the sample is mainly adventitious. This provides clear evidence of the laser removing a majority of the remaining organic vehicle. Due to this, the O1s peak also shifts 3.3 eV to a lower binding energy, signifying a removal of C=O bonds associated with the nitrocellulose binder and, moving to a pure metal-oxygen bond. Consistent with a lack of evidence of metallic tin being detected via XRD, XPS measurements also suggest the only tin present is in the form of tin oxide. The indium 3d peaks are also broad providing evidence that the bulk of the indium is in the In_2O_3 configuration. The indium Auger peaks InMN1 also provide no clear evidence of metallicity or reduction, however, any surface metals are expected to oxidize readily in air. The binding energies for both the tin and indium do decrease slightly with asymmetric peaks, indicating a potential decrease in oxidation number for the indium tin oxide and multiple oxidation states being present. The XPS atomic percentage ratios of indium to tin in the oven cured sample in comparison to the laser processed sample are, 10.09:1 to 5.64:1 respectively giving a 1.79x difference. For the SEM based EDX data as shown in Fig. 3(c), the ratio alters from 7.33:1 to 3.38:1 between oven and laser processed samples respectively, showing a 2.16x change. Between the two techniques, comparing surface (by XPS) and bulk (by SEM/EDX), there is a common increase in tin content. These changes in the atomic ratio, can typically be due to either elemental migration of dopant to the surface of the particles or migration of within the film itself, sinking to a depth greater than the penetration depth of EDX and XPS. Considering, the carrier concentration decreases in the ITO nanowires, this phenomenon can be described by a migration of dopant towards the surface of the crystallites. This provides evidence of a

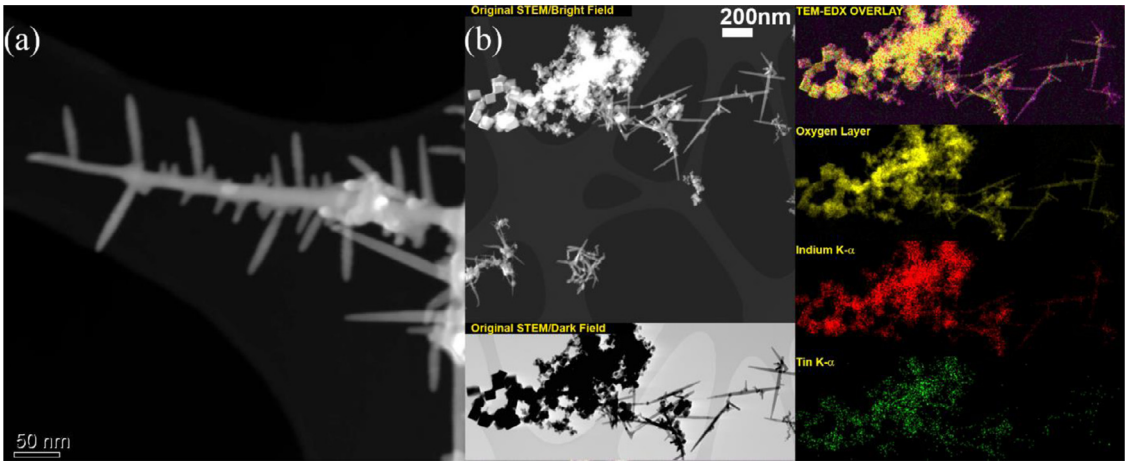

Fig.. 4. Transmission Electron Microscope Analysis (a) An image of a 10 W Laser Processed ITO Nanowire Structure (b) STEM dark and bright field images of nanowires, nano-cubes, and fine particles with associated EDX mapping analysis.

Table 1
Sn:In atomic ratios of laser grown ITO morphologies.

Area	Sn	In
Nanowires	1	6.42
Cubic	1	6.43
Fine Particles	1	6.43

migration of tin from the particle interior to the exterior with the possibility of SnO_2:In_2O_3 phase separation.

To determine the actual phase, composition change and crystal structure of the formed ITO nanowires, and to provide insight into the formation process, transmission electron microscopy (TEM) was performed on the nanowires. The 10 W film was selected for TEM analysis due to the extremely fine size of nanowires being beyond the routine resolution limit of SEM analysis. TEM images and elemental maps were recorded for the ITO nanowires (Fig. 4). From the TEM analysis, it was evident that most of the film had converted to nanowires of varying amounts with fine particles and nano-cubes being relatively difficult to find. A typical nanowire at 10 W processing power had a width of approximately 10 – 20 nm with lengths of 500 – 800 nm, with a mixture of branching needles.

For the ITO nanowires, TEM-EDX mapping (Fig. 4(b)) was performed on a selection of particles which show the growth process of the nanowire. It can be observed that the original cubic particles convert into structures formed of fine particles, these then reform into wire and whisker like structures. EDX point analysis was performed on each of these structures shown in Fig. 4(b) and is displayed in Table 1. For the nanowires, cubic and fine particles a 6.42:1, 6.43:1 and 6.43:1 indium to tin ratio was observed. This indicates that, post laser processing, the overall composition remains uniform and consistent.

As suggested in the XRD data, there is evidence of a reduction process taking place during the laser processing, driven by a carbothermal reduction of the metal oxides via the carbon heavy ink vehicle. The EDX data shown in Fig. 4(b) shows that for the range of particles seen, the material composition is consistent. This indicates that the change in composition shown in Fig. 2(d) occurs in the early stages of the laser treatment.

Selected area diffraction patterns (Fig. S8) were taken of the ITO nanowires to determine whether the wires are formed through sintering, fusing or crystal growth. The selected area electron diffraction (SAED) pattern displays polycrystalline behavior showing that the rods are not single crystal. No regions of single ITO nanowires could be found in the TEM so the SAED pattern was taken of a region with multiple nanowires but no other particle morphologies. This showed bright spots in a pattern indicating a cubic crystal structure matching the structure of ITO, the brightness of the spots indicates the nanowires are highly crystalline. However, polycrystallinity is observed due to the large number of particles in the aperture of the TEM. This, combined with the crystallite size changes discussed earlier, suggests that although there is crystallite growth, the nanowire growth is largely due to the fusion of crystallites.

Overall, the data presented in this paper suggest the high energies of the laser treatments of 10 W or more combined with the heavy organic loading of the ink vehicle creates an environment where the carbon acts as a reducing agent. This can be deduced by the presence of metallic indium in the XRD data, and the oxygen deficiency of the nanowires in the EDX data. The SEM and TEM imaging indicate that the microparticles are broken down into nanoparticles by the laser, possibly as a result of this reduction. The SAED patterns then indicate these fine particles then fuse together, building the nanowires shown. A possible mechanism for this process is that as the carbon and oxygen burn off as CO_2, the metal oxide particles reduce into oxygen-deficient or metallic intermediates. As the ITO undergoes a re-oxidation into its previous state, the fine particles combine, assembling into nanowires and hierarchical 3D nanowires. In order to determine whether the reduction is driven by the addition of carbon or a different factor, a second ink was formulated with the addition of carbon nanotubes. Upon laser processing the ink an X-ray diffraction pattern was taken in order to detect any reduction of the metal oxides. A secondary phase (Fig. S9) can be seen alongside the typical ITO pattern. This phase correlates to the indium / tin alloy, In_3Sn (PDF 96–153–8884) suggesting that the addition of the extra carbon increases the levels of ITO reduction. This data therefore confirms the laser is causing is a carbothermal reduction.

This paper has shown that it is possible to grow ITO nanowires through printing and laser processing, adding to the arsenal of tools which can be used for electronics manufacturing. As a brief example of printing and patterning an interdigitated structure was printed, and laser processed and can be seen in Fig. 3a (inset). Interdigitation is a commonly used structure in many applications, which include sensors [22–24]. The ability to print and pattern ITO nanowires into functional structures such as this one, enables, in future work, the manufacturing of sensors which incorporate sens-

ing materials without the need for etching, reducing the waste of materials, the amount of energy needs to process the materials and the amount of steps and errors caused by this during manufacturing. Future work should also focus on further optimization of the process in order to achieve denser, lower resistivity nanowire films.

5. Conclusion

In conclusion, we have shown that by formulating carbon heavy indium tin oxide microparticle inks, the indium tin oxide can undergo a controlled nanostructure change, after being processed with laser radiation. After a full materials characterization study, the evidence shows that the laser induces a carbothermal reduction synthesis, burning off the carbon-based vehicle as CO_2 and partially reducing to metal. This metal undergoes re-oxidation, converting cubic particles into nanostructures dependent on the material's crystal structure. Compared to the original material's bulk resistivity, using this laser process allows the manufacture of printed indium tin oxide patterns at 40.47% bulk conductivity, compared to the base ink which provides 0.88% of bulk conductivity. These findings enable further research into applying this rapid manufacturing process to a vast array of metal oxides to provide a range of nanostructured materials which have applications in a large number of fields including electronics manufacturing, sensor development and frequency selective surfaces.

Data availability

Upon publication of this article, data used for the creation of this manuscript can be found at 10.17028/rd.lboro.12793895.

Declaration of Competing Interest

The authors have no conflicts of interest to declare.

Acknowledgments

This research was funded as part of EPSRC grant (EP/L017709/1) investigating "Sustainable Manufacturing of Transparent Conducting Oxide (TCO) Inks and Thin Films" - a collaboration between Loughborough University's Design School, the Department of Chemistry, Wolfson School of Mechanical Engineering and Manufacturing and University College London (UCL). The authors also greatly appreciate the assistance of the industrial partners involved in this collaborative research program. The authors acknowledge and appreciate the use of metrology facilities guided by Jagpal Singh within the School of Mechanical, Electrical and Manufacturing Engineering, Loughborough University. The authors also acknowledge the help and expertise of Dr Pat Cropper in acquiring XPS data with the facilities of the Loughborough Materials Characterization Centre.

Author contributions

Dr J. R. McGhee and Dr A. Goulas performed and developed the conceptualization, methodology, data curation, the formal analysis, and investigation. Dr D. J. Southee, D. S. Engstrøm, Dr. J. Wang and Dr. D. A. Hutt aided in conceptualization, methodology development and data analysis. Dr. P. S. A. Evans, Dr. J. S. Sagu and Dr. Z. Zhou aided in methodology development and investigation. Dr D. J. Southee, Dr D. A. Hutt, Professor K. G. U. Wijayantha, Professor P. Conway and Professor C. Carmalt provided funding acquisition, supervision, resources, project administration and conceptualization. Dr J. R. McGhee wrote the original draft and all authors wrote and revised the manuscript.

Supplementary materials

Supplementary material associated with this article can be found, in the online version, at doi:10.1016/j.apmt.2020.100835.

References

[1] R. Yan, D. Gargas, P. Yang, Nanowire photonics, Nat. Photonics 3 (Oct.) (2009) 569.
[2] J.-P. Colinge, et al., Nanowire transistors without junctions, Nat. Nanotechnol. 5 (Feb.) (2010) 225.
[3] T.W. Larsen, et al., Semiconductor-nanowire-based superconducting qubit, Phys. Rev. Lett. 115 (Sep. (12)) (2015) 127001.
[4] S. Gazibegovic, et al., Epitaxy of advanced nanowire quantum devices, Nature 548 (Aug.) (2017) 434.
[5] M.E. Stewart, et al., Nanostructured plasmonic sensors, Chem. Rev. 108 (Feb. (2)) (2008) 494–521.
[6] A. Umar, J.-H. Lee, R. Kumar, O. Al-Dossary, A.A. Ibrahim, S. Baskoutas, Development of highly sensitive and selective ethanol sensor based on lance-shaped CuO nanostructures, Mater. Des. 105 (2016) 16–24 pp.
[7] A. Dey, Semiconductor metal oxide gas sensors: a review, Mater. Sci. Eng. B Solid-State Mater. Adv. Technol. 229 (2018) 206–217 pp.
[8] F. Patolsky, C.M. Lieber, Nanowire nanosensors, Mater. Today 8 (4) (2005) 20–28 pp.
[9] Y. Cui, C.M. Lieber, Functional nanoscale electronic devices assembled using silicon nanowire building blocks, Science (80-.) 291 (5505) (2001) 851–853.
[10] X. Duan, Y. Huang, Y. Cui, J. Wang, C.M. Lieber, Indium phosphide nanowires as building blocks for nanoscale electronic and optoelectronic devices, Nature 409 (6816) (2001) 66–69.
[11] Z.L. Wang, J. Song, Piezoelectric nanogenerators based on zinc oxide nanowire arrays, Science (80-.) 312 (5771) (2006) 242–246.
[12] K. Ellmer, Past achievements and future challenges in the development of optically transparent electrodes, Nat. Photonics 6 (12) (2012) 809–817.
[13] Q. Li, et al., 3D ITO-nanowire networks as transparent electrode for all-terrain substrate, Sci. Rep 9 (1) (2019) 4983.
[14] D.-W. Kim, et al., Highly conductive coaxial SnO_2-In_2O_3 heterostructured nanowires for Li ion battery electrodes, Nano Lett. 7 (10) (2007) 3041–3045.
[15] S. Ye, A.R. Rathmell, Z. Chen, I.E. Stewart, B.J. Wiley, Metal nanowire networks: the next generation of transparent conductors, Adv. Mater. 26 (39) (2014) 6670–6687.
[16] Y.H. Kim, H. Koo, M.S. Kim, S.-.D. Jung, Iridium oxide on indium-tin oxide nanowires: an all metal oxide heterostructured multi-electrode array for neuronal interfacing, Sensors Actuators B Chem. 273 (2018) 718–725.
[17] J.A. Hernandez, J. Carpena-Nunez, L.F. Fonseca, M.T. Pettes, M.J. Yacaman, A. Benitez, Thermoelectric properties and thermal tolerance of indium tin oxide nanowires, Nanotechnology 29 (Sep. (36)) (2018) 364001.
[18] C. Liu, et al., High-density, ordered ultraviolet light-emitting ZnO nanowire arrays, Adv. Mater. 15 (10) (2003) 838–841.
[19] S.H. Ko, et al., Nanoforest of hydrothermally grown hierarchical ZnO nanowires for a high efficiency dye-sensitized solar cell, Nano Lett. 11 (2) (2011) 666–671.
[20] Y. Zhou, C. Gao, Y. Guo, UV assisted ultrasensitive trace NO_2 gas sensing based on few-layer MoS_2 nanosheet-ZnO nanowire heterojunctions at room temperature, J. Mater. Chem. A 6 (22) (2018) 10286–10296.
[21] M. Ha, S. Lim, J. Park, D.-S. Um, Y. Lee, H. Ko, Bioinspired interlocked and hierarchical design of ZnO nanowire arrays for static and dynamic pressure-sensitive electronic skins, Adv. Funct. Mater. 25 (19) (2015) 2841–2849.
[22] D. Ko, et al., Chemical sensing properties of indium-tin-oxide (ITO) printed films fabricated on biodegradable plastics, AIP Adv. 10 (Apr. (4)) (2020) 45228.
[23] C.R. Zamarreño, M. Hernaez, I. Del Villar, I.R. Matias, F.J. Arregui, Sensing properties of ITO coated optical fibers to diverse VOCs, Procedia Eng. 5 (2010) 653–656.
[24] J.R. McGhee, J.S. Sagu, D.J. Southee, K.G.U. Wijayantha, Humidity sensing properties of transparent sputter-coated indium-tin oxide and printed polymer structures, IEEE Sens. J. 18 (18) (2018).
[25] J.R. McGhee, M. Sinclair, D.J. Southee, K.G.U. Wijayantha, Strain sensing characteristics of 3D-printed conductive plastics, Electron. Lett. 54 (9) (2018).
[26] Y. Mao, S. Banerjee, S.S. Wong, Large-scale synthesis of single-crystalline perovskite nanostructures, J. Am. Chem. Soc. 125 (Dec. (51)) (2003) 15718–15719.
[27] A. Biswas, I.S. Bayer, A.S. Biris, T. Wang, E. Dervishi, F. Faupel, Advances in top–down and bottom–up surface nanofabrication: techniques, applications & future prospects, Adv. Colloid Interface Sci. 170 (1) (2012) 2–27.
[28] F. Panciera, et al., Synthesis of nanostructures in nanowires using sequential catalyst reactions, Nat. Mater. 14 (8) (2015) 820–825.
[29] J. Yang, T. Mori, M. Kuwabara, Mechanism of carbothermic reduction of hematite in hematite carbon composite pellets, ISIJ Int. 47 (10) (2007) 1394–1400.
[30] M.O. Orlandi, P.H. Suman, R.A. Silva, E.P.S. Arlindo, Eds. Cham: Springer International Publishing, 2017, pp. 43–67.
[31] L. Yan, A. Uddin, H. Wang, ZnO Tetrapods: synthesis and applications in solar cells, Nanomater. Nanotechnol. 5 (Jan.) (2015) 19.
[32] J.R. McGhee, R.B. Middlemiss, D.J. Southee, K.G.U. Wijayantha, P.S.A. Evans, Flexible, all metal-oxide capacitors for printed electronics, in: 2018 IEEE 13th Nanotechnology Materials and Devices Conference (NMDC), 2018, pp. 1–4.
[33] S. Yang, et al., Influence of base pressure on property of sputtering deposited ITO film, J. Mater. Sci. Mater. Electron. 30 (14) (2019) 13005–13012.